MATHEMATICAL MODELING AND COMPUTING, Vol. 11, No. 1, pp. 27–36 (2024)

Impact of magnetohydrodynamic on hybrid nanofluid flow with slip and heat source over an exponentially stretchable/shrinkable permeable sheet

Radzi N. A. M.[1], Wahid N. S.[1], Som A. N. M.[3], Arifin N. M.[1,2]

[1] *Department of Mathematics and Statistics, Faculty of Science, University Putra Malaysia, 43400 UPM Serdang, Selangor, Malaysia*
[2] *Institute for Mathematical Research, University Putra Malaysia, 43400 UPM Serdang, Selangor, Malaysia*
[3] *Centre of Foundation Studies for Agriculture Sciences, University Putra Malaysia, 43400 UPM Serdang, Selangor, Malaysia*

(Received 25 June 2023; Revised 8 November 2023; Accepted 8 November 2023)

This research examines the hybrid nanofluid alumina-copper/water flow over a permeable sheet, considering slip, magnetohydrodynamics, and heat source. To analyze the system, the model is transformed into nonlinear ordinary differential equations (ODEs) via the similarity transformation. Numerical solutions are attained through the implementation of the bvp4c function in MATLAB. The study analyzes velocity and temperature profiles, local skin friction, and Nusselt number for various parameters. Moreover, the impact of magnetohydrodynamics on the system is explored. Increasing the magnetic parameter leads to an enlargement of the boundary layer thickness and an elevation in the skin friction coefficient. Overall, this study sheds light on the complex behavior of hybrid nanofluid flows and provides valuable insights into the effects of slip, magnetohydrodynamics, and heat source on the model while also presenting a validated model showcasing the compelling enhancement of heat transfer through the incorporation of copper into alumina nanofluid.

Keywords: *magnetohydrodynamic; hybrid nanofluid; heat source; stretching/shrinking.*
2010 MSC: 35Q35, 76A02, 76D10, 76D55, 80A20 **DOI:** 10.23939/mmc2024.01.027

1. Introduction

The investigation conducted by Choi [1] in 1995 marked a significant milestone in the study of nanofluids, as Taylor et al. [2] define them as noteworthy products within the realm of nanotechnology. Nanofluids, consisting of a suspension of nanoparticles in a base fluid, initially received attention primarily for measuring and modeling their fundamental thermophysical properties. However, recent research endeavors have expanded the exploration of nanofluids to encompass their performance in various practical applications, including heat exchangers and electronic cooling systems [3]. The emergence of nanofluid has then introduced a new novel type of nanofluid that combines different nanoparticles into one specific base fluid, with the aim to enhance heat transfer properties [4]. A wealth of experimental and numerical studies conducted by researchers consistently substantiate that hybrid nanofluids exhibit superior heat transfer rates compared to both pure fluids and conventional nanofluids. Several studies and reviews on the hybrid nanofluid can be contemplated in the following references [5–11].

The magnetohydrodynamic effect is significant in fluid dynamic studies, particularly when examining conducting fluids near solid surfaces. The magnetic field affects flow characteristics and heat transfer within the boundary layer. This interaction modifies flow patterns, boundary layer thickness, and heat transfer rates, impacting overall fluid dynamics near the surface. Understanding and analyzing this effect offers insights for controlling and optimizing flow and heat transfer in engineer-

The authors acknowledge the grant from UPM (GP-GPB 9711400).

ing applications, including cooling systems, aerodynamics, and energy conversion systems. Recently, numerous researchers have incorporated the magnetohydrodynamic effect into their investigation of hybrid nanofluid boundary layer flow. For instance, in the numerical study on Casson hybrid nanofluid past a stretch/shrink sheet with radiation, Mahabalshwar et al. [12] have implemented the magnetohydrodynamic effect. Later, Mehesh et al. [13] scrutinized the radiative magnetohydrodynamic of a hybrid nanofluid with viscous dissipation over a porous sheet. They found out that the increment of magnetohydrodynamic has reduced the fluid temperature. The magnetohydrodynamic effect has also been considered by Wahid et al. [14] in their study on the radiative-mixed convective hybrid nanofluid over a shrink-permeable inclined plate. It is elucidated that the heat transfer in their model can be improved when using a stronger magnetohydrodynamic effect. In the study of hybrid nanofluid flow past an exponentially stretched/shrunk surface within a porous space, Jaafar et al. [15] also implemented the magnetohydrodynamic effect. In their case, the magnetohydrodynamic is recommended to enlarge the skin friction in the boundary layer flow. Recently, Patel et al. [16] concluded that the magnetohydrodynamic effect can be used to hinder boundary layer separation.

Recognizing the importance of hybrid nanofluids in conjunction with magnetohydrodynamic and heat source, our study is inspired to build upon the study conducted by Waini et al. [10] and Wahid et al. [11]. In this research endeavor, we aim to investigate the impact of magnetohydrodynamic on the hybrid nanofluid flow over a permeable stretchable/shrinkable sheet with slip and heat source. We have seen that the work by Wahid et al. [10] did not include the magnetohydrodynamic effect, while the study by Waini et al. [10] did not include the heat source and slip effects. Hence, we want to bridge the model gap by simultaneously implementing these effects together toward hybrid nanofluid flow over an exponentially permeable stretchable/shrinkable sheet.

2. Mathematical model

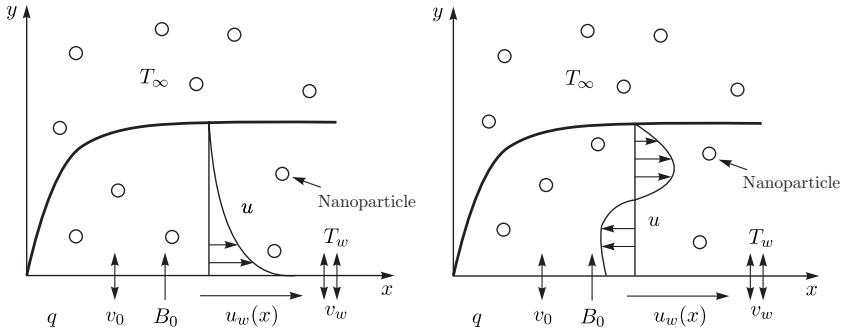

a Stretching sheet ($\lambda > 0$) ***b*** Shrinking sheet ($\lambda < 0$)

Fig. 1. The physical models.

Figure 1 shows a hybrid alumina-copper/water nanofluid boundary layer flow over an exponentially permeable stretchable/shrinkable sheet with a heat source, slip, and magnetohydrodynamic effects, where x and y are the Cartesian coordinates such that the x-axis is located along the stretch/shrink sheet and the y-axis is normal to the sheet. The velocities are u (x-direction) and v (y-direction), while T is temperature. Some assumptions are made such as [10,11]:

- the magnetic field factor imposed on the y-direction is $B_m(x) = B_0\, e^{\frac{x}{2L}}$, where B_0 is the magnetic constant;
- the heat source factor is $q = q_0\, e^{\frac{x}{L}}$, where q_0 is the heat source constant;
- the sheet temperature is $T_w = T_\infty + T_0\, e^{\frac{x}{2L}}$ with T_0 as the temperature constant and T_∞ as the ambient temperature;
- the velocity slip factor is $A^* = A_1\, e^{-\frac{x}{2L}}$, and the thermal slip factor is $B^* = B_1 e^{-\frac{x}{2L}}$ [17];
- the sheet velocity is $u_w(x) = c\, e^{\frac{x}{L}}$, where the shrink constant for the sheet is $\lambda < 0$, the stretch constant is $\lambda > 0$, and $\lambda = 0$ is when the sheet is not stretch/shrink;
- the mass transfer velocity is $v_w(x) = -\sqrt{\frac{c\nu_f}{2L}} e^{\frac{x}{2L}} S$, where $S > 0$ is for suction and $S < 0$ is for injection;
- for the hybrid nanofluid, the considered formulations are presented in Table 1 [10,11,18], while the related values are tabulated in Table 2 [10,11,19–22].

Table 1. Formulations for the thermophysical properties.

Properties	Formulations
Density	$\rho_{hnf} = \rho_{s1}\phi_{s1} + \rho_{s2}\phi_{s2} + \rho_f(1-\phi_{hnf})$, where $\phi_{hnf} = \phi_{s1} + \phi_{s2}$
Heat capacity	$(\rho\, C_p)_{hnf} = (\rho\, C_p)_{s1}\phi_{s1} + (\rho\, C_p)_{s2}\phi_{s2} + (\rho\, C_p)_f(1-\phi_{hnf})$
Dynamic viscosity	$\frac{\mu_{hnf}}{\mu_f} = \frac{1}{(1-\phi_{hnf})^{2.5}}$
Thermal conductivity	$\frac{k_{hnf}}{\mu_f} = \frac{2k_f + \frac{\phi_{s1}k_{s1}+\phi_{s2}k_{s2}}{\phi_{hnf}} + 2\phi_{s1}k_{s1} + \phi_{s2}k_{s2}}{2k_f - (\phi_{s1}k_{s1}+\phi_{s2}k_{s2}) + \frac{\phi_{s1}k_{s1}+\phi_{s2}k_{s2}}{\phi_{hnf}} + \phi_{hnf}k_f}$
Electrical conductivity	$\sigma_{hnf} = \frac{\sigma_{s2}+2\sigma_{nf}-2\phi_2(\sigma_{nf}-\sigma_{s2})}{\sigma_{s2}+2\sigma_{nf}+\phi_2(\sigma_{nf}-\sigma_{s2})}(\sigma_{nf})$, where $\sigma_{nf} = \frac{\sigma_{s1}+2\sigma_f-2\phi_{s1}(\sigma_f-\sigma_{n1})}{\sigma_{s1}+2\sigma_f+\phi_{s1}(\sigma_f-\sigma_{s1})}(\sigma_f)$

Here in the table, ϕ_{s1} is for alumina (Al_2O_3) volume fraction and ϕ_{s2} is for copper (Cu) volume fraction, while the subscript of 'hnf' refers to hybrid nanofluid, 'nf' refers to nanofluid, and 'f' refers to base fluid (water).

Table 2. Thermophysical properties.

Properties	Alumina	Copper	Water
ρ ($\mathrm{kg\,m^{-3}}$)	3970	8933	997.1
k ($\mathrm{W\,m^{-1}K^{-1}}$)	40	400	0.613
C_p ($\mathrm{J\,kg^{-1}K^{-1}}$)	765	385	4179
σ ($\mathrm{S\,m^{-1}}$)	3.69×10^7	5.96×10^7	0.05
Pr	–	–	6.2

Therefore, according to the given assumptions, the formulations are as follows (see Waini et al. [10], Wahid et al. [11]):

- Continuity equation:

$$\frac{\partial u}{\partial x} + \frac{\partial v}{\partial y} = 0; \tag{1}$$

- Momentum equation:

$$u\frac{\partial u}{\partial x} + v\frac{\partial u}{\partial y} = \frac{\mu_{hnf}}{\rho_{hnf}}\frac{\partial^2 u}{\partial y^2} - \frac{\sigma_{hnf}}{\rho_{hnf}}B_m^2 u; \tag{2}$$

- Energy equation:

$$u\frac{\partial T}{\partial x} + v\frac{\partial T}{\partial y} = \frac{k_{hnf}}{(\rho\, C_p)_{hnf}}\frac{\partial^2 T}{\partial y^2} + \frac{q}{(\rho\, C_p)_{hnf}}(T - T_\infty); \tag{3}$$

- Boundary conditions:

$$u = u_w(x)\lambda + A^*\frac{\mu_{hnf}}{\rho_{hnf}}\frac{\partial u}{\partial y}, \quad v = v_w, \quad T = T_w(x) + B^*\frac{\partial T}{\partial y} \quad \text{at} \quad y = 0,$$
$$u \to 0, \quad T \to T_\infty \quad \text{as} \quad y \to \infty. \tag{4}$$

Then, the following stream function and similarity variables are introduced [10, 11]:

$$\eta = y\, e^{x/2L}\sqrt{\frac{c}{2\nu_f L}}, \quad \psi = e^{x/2L}\sqrt{2\nu_f L c}f(\eta), \quad u = \frac{\partial \psi}{\partial y}, \quad v = -\frac{\partial \psi}{\partial x}, \quad \theta = \frac{T - T_\infty}{T_w - T_\infty}. \tag{5}$$

After the transformation, the continuity equation is satisfied, while the other equations become:

$$\frac{\mu_{hnf}/\mu_f}{\rho_{hnf}/\rho_f}f''' + ff'' - 2f'^2 - \frac{\sigma_{hnf}/\sigma_f}{\rho_{hnf}/\rho_f}Mf' = 0, \tag{6}$$

$$\left(\frac{k_{hnf}}{k_f}\right)\frac{1}{\mathrm{Pr}}\theta'' + \left(f\theta' - f'\theta\right)\frac{(\rho\, C_p)_{hnf}}{(\rho\, C_p)_{hnf}} + \beta\theta = 0, \tag{7}$$

subject to,

$$f(0) = S, \quad f'(0) = \lambda + A\, f''(0), \quad \theta(0) = 1 + B\,\theta'(0), \quad f'(\infty) \to 0, \quad \theta(\infty) \to 0, \tag{8}$$

where $M = \frac{2\sigma_f {B_0}^2 L}{c\rho_f}$ is the magnetic parameter, $\mathrm{Pr} = \frac{\nu_f}{\alpha_f}$ is the Prandtl number such that $\alpha = \frac{k_f}{(\rho Cp)_f}$, $\beta = \frac{2Lq_0}{(\rho Cp)_f c}$ is the heat source parameter, $A = A_1\left(\frac{\mu_{hnf}}{\rho_{hnf}}\right)\sqrt{\frac{c}{2\nu_f L}}$ is the velocity slip parameter, and $B = B_1\sqrt{\frac{c}{2\nu_f L}}$ is the thermal slip parameter.

The physical quantities involved are local skin friction, C_f and Nusselt number, Nu_x [11]:

$$C_f = \frac{\mu_{hnf}}{\rho_f}\frac{1}{u_w^2}\left(\frac{\partial u}{\partial y}\right)_{y=0}, \quad \mathrm{Nu}_x = \frac{k_{hnf}}{k_f}\frac{-2L}{T_w - T_\infty}\left(\frac{\partial T}{\partial y}\right)_{y=0}. \tag{9}$$

After transformation, we should get

$$(\mathrm{Re}_x)^{1/2}C_f = \frac{\mu_{hnf}}{\mu_f}f''(0), \quad (\mathrm{Re}_x)^{-1/2}\mathrm{Nu}_x = -\frac{k_{hnf}}{k_f}\theta'(0), \tag{10}$$

where $\mathrm{Re}_x = \frac{2Lu_w}{\nu_f}$ is the local Reynolds number.

3. Results and discussion

The magnetic effect of magnetohydrodynamic on alumina–copper/water flow over a stretchable/shrinkable sheet with slip effect and heat source are presented graphically and discussed in this section. The suction effect is a method of boundary layer control to reduce drag on bodies in an external flow and it helps in reducing energy losses in the system. With the existence of a velocity slip parameter, the friction between sheets is decreased, and wasteful use of energy is prevented. The heat source can control the forming heat internally and externally.

Table 3. Comparison value of results with previous studies.

Solutions	Present Results	Waini et al. [10]	Wahid et al. [11]
First, $f''(0)$	2.390813633	2.390814	2.39081363
Second, $f''(0)$	-0.972247455	-0.972247	-0.97212886
First, $-\theta'(0)$	1.771237338	1.771237	1.771237307
Second, $-\theta'(0)$	0.848315747	0.848316	0.84774827

The ODEs system has been solved and the solutions were obtained numerically by bvp4c in MATLAB software. Table 3 shows the comparison results for the case when $M = A = B = \beta = \phi_{s1} = \phi_{s2} = 0$, $\mathrm{Pr} = 0.7$, $S = 3$, and $\lambda = -1$ with the previous studies. Thus, in this comparison, the present results are within the range of the results provided in the previous studies, thus, the technique for obtaining the results can be guaranteed and decent.

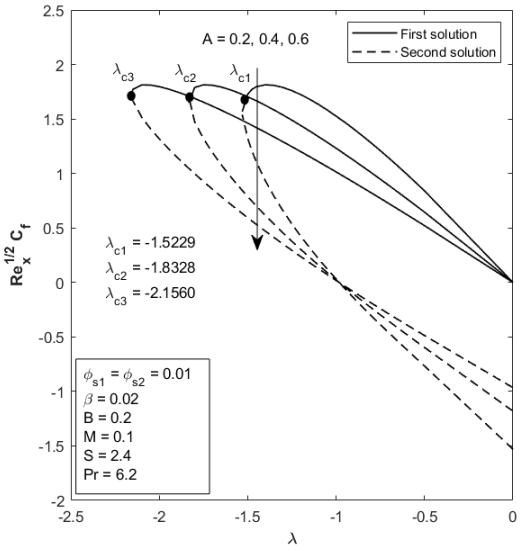

Fig. 2. $\mathrm{Re}_x^{1/2}C_f$ with λ for several A.

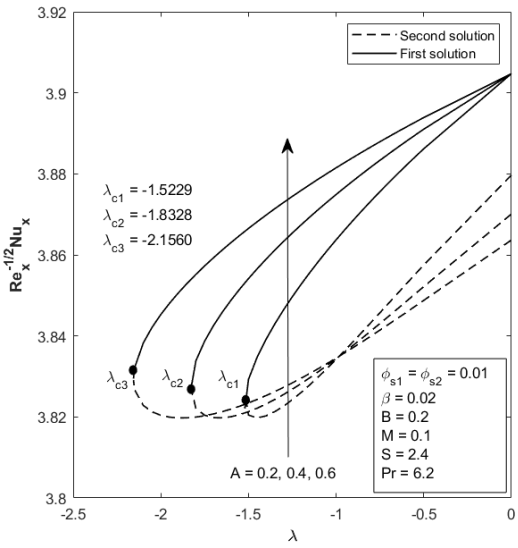

Fig. 3. $\mathrm{Re}_x^{-1/2}\mathrm{Nu}_x$ with λ for several A.

Figures 2 and 3 show the impact of several values of A on $(\mathrm{Re}_x)^{1/2}C_f$ and $(\mathrm{Re}_x)^{-1/2}\mathrm{Nu}_x$, when $\lambda < 0$, $\phi_{s1} = \phi_{s2} = 0.01$, $\beta = 0.02$, $B = 0.2$, $M = 0.1$, and $S = 2.4$. From the figures, $(\mathrm{Re}_x)^{1/2}C_f$ diminishes for both solutions, when A enlarges with $\lambda < 0$ but the trend is not consistent for the second solution when $\lambda > -1$. Meanwhile, $(\mathrm{Re}_x)^{-1/2}\mathrm{Nu}_x$ enhances when A enlarges for both solutions, except for the second solution, when $\lambda > -1$. The laminar flow phase is seen to be maintained longer if A enlarges.

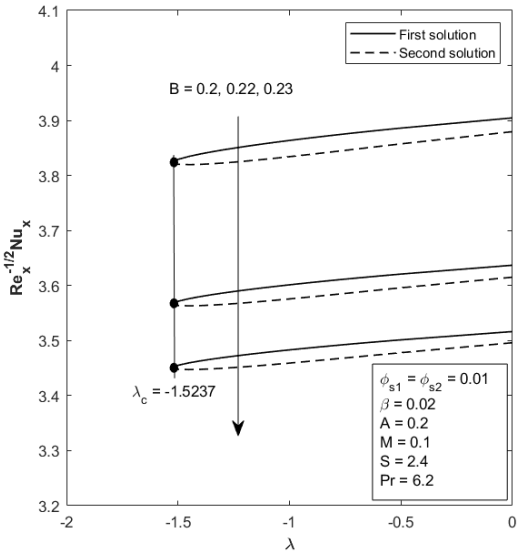

Fig. 4. $\mathrm{Re}_x^{-1/2}\mathrm{Nu}_x$ with λ for several B.

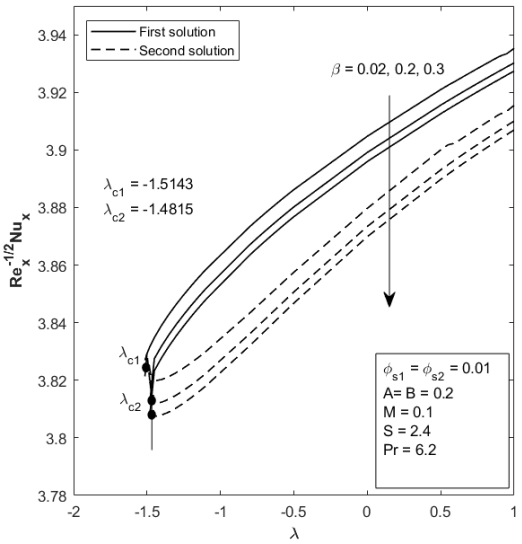

Fig. 5. $\mathrm{Re}_x^{-1/2}\mathrm{Nu}_x$ with λ for several β.

Figure 4 shows the impact of several values of B on $(\mathrm{Re}_x)^{-1/2}\mathrm{Nu}_x$, when $\lambda < 0$, $\phi_{s1} = \phi_{s2} = 0.01$, $\beta = 0.02$, $A = 0.2$, $M = 0.1$, and $S = 2.4$. It is seen that $(\mathrm{Re}_x)^{-1/2}\mathrm{Nu}_x$ diminishes if the value of B enlarges. After all, this parameter is not suitable to control the flow phase since the critical point is not changeable due to the changing value of B.

Figure 5 shows the impact of several values of β on $(\mathrm{Re}_x)^{-1/2}\mathrm{Nu}_x$, when $\lambda < 1$, $\phi_{s1} = \phi_{s2} = 0.01$, $A = B = 0.2$, $M = 0.1$, and $S = 2.4$. The figure shows that as the value of β enlarges, $(\mathrm{Re}_x)^{-1/2}\mathrm{Nu}_x$ reduces regardless of when the sheet is stretched or shrunk.

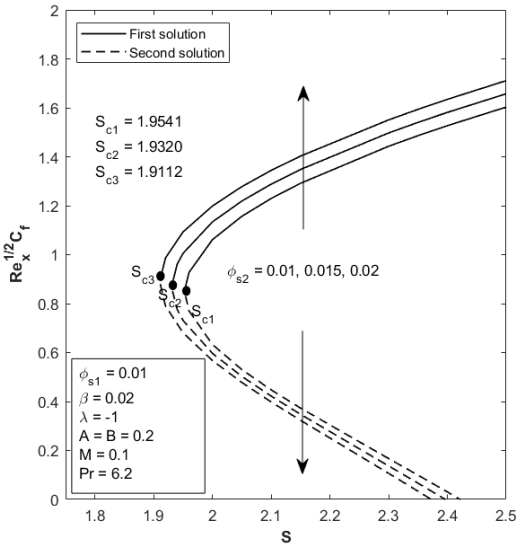

Fig. 6. $\mathrm{Re}_x^{1/2}C_f$ with S for several ϕ_{s2}.

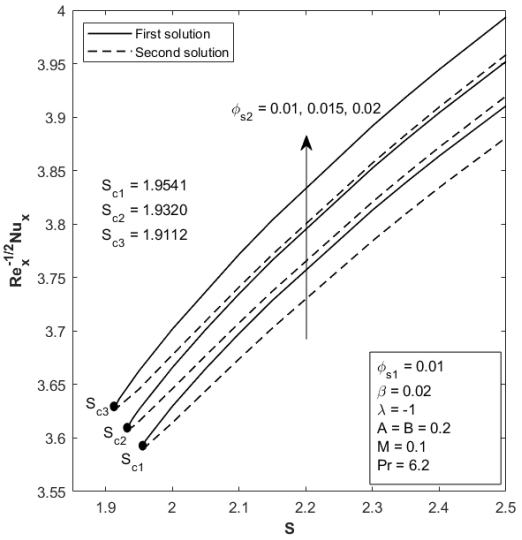

Fig. 7. $\mathrm{Re}_x^{-1/2}\mathrm{Nu}_x$ with S for several ϕ_{s2}.

Figures 6 and 7 show the impact of several values of ϕ_{s2} on $(\mathrm{Re}_x)^{1/2}C_f$ and $(\mathrm{Re}_x)^{-1/2}\mathrm{Nu}_x$ against $S < 2.5$ with $\phi_{s1} = 0.01$, $\beta = 0.02$, $\lambda = -1$, $A = B = 0.2$, and $M = 0.1$. From the figure, $(\mathrm{Re}_x)^{1/2}C_f$ is seen to enhance when larger ϕ_{s2} is used except for the second solution. Also, the enlargement of ϕ_{s2} enhances $(\mathrm{Re}_x)^{-1/2}\mathrm{Nu}_x$ for both solutions and hinders the layer separation. This result proves that the suitably higher insertion of ϕ_{s2} enhances the heat transfer which also satisfies the judgment that the hybrid nanofluid has the ability to enhance the heat transfer.

Figures 8 and 9 show the impact of several values of M on $(\mathrm{Re}_x)^{1/2}C_f$ and $(\mathrm{Re}_x)^{-1/2}\mathrm{Nu}_x$ against $\lambda < 1$ with $\phi_{s1} = \phi_{s2} = 0.01$, $\beta = 0.02$, $A = B = 0.2$, and $S = 2.4$. From the figures, as the value of M

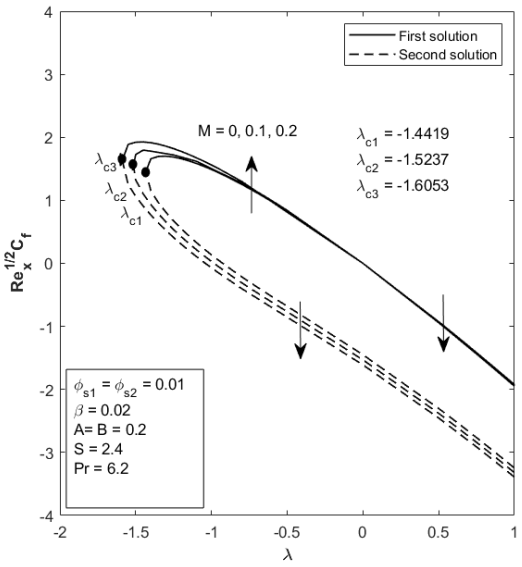

Fig. 8. $\mathrm{Re}_x^{1/2}C_f$ with λ for several M.

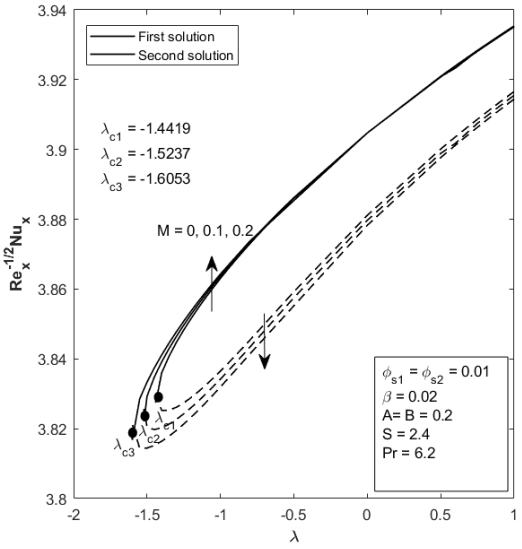

Fig. 9. $\mathrm{Re}_x^{-1/2}\mathrm{Nu}_x$ with λ for several M.

enlarges, the first solution enhances in the shrinkable case and diminishes in the stretchable case, while the second solution diminishes $(\mathrm{Re}_x)^{1/2}C_f$ for both cases. Besides, the first solution of $(\mathrm{Re}_x)^{-1/2}\mathrm{Nu}_x$ enhances when the value of M enlarges but not for the second solution. The position of the critical point shows that the larger M could maintain the laminar flow phase better compared to the lesser M.

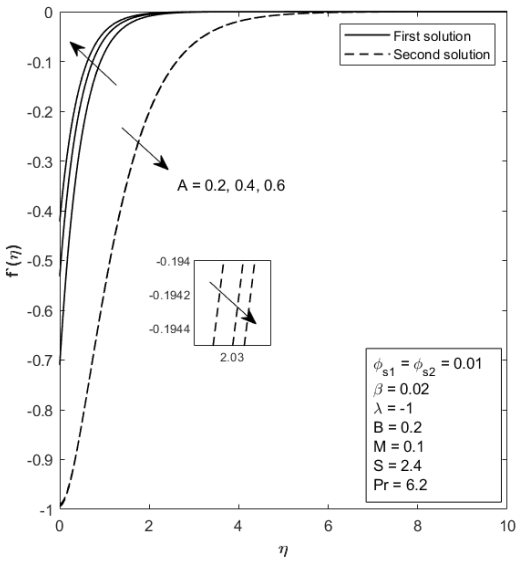

Fig. 10. Velocity profile for several A.

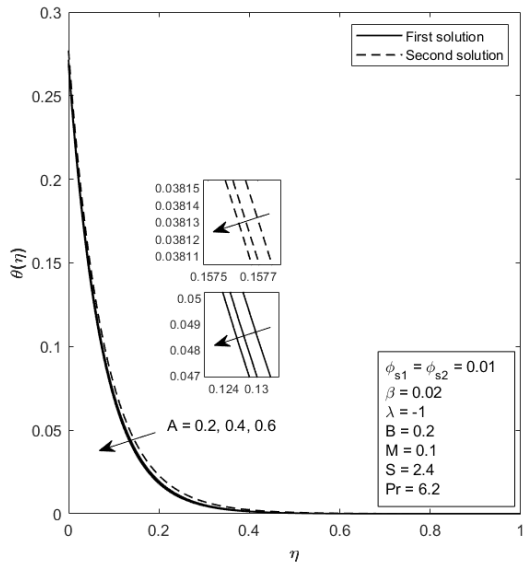

Fig. 11. Temperature profile for several A.

Figures 10 and 11 show the impact of several values of A on the velocity profile $f'(\eta)$ and temperature profile $\theta(\eta)$, when $\phi_{s1} = \phi_{s2} = 0.01$, $\beta = 0.02$, $\lambda = -1$, $B = 0.2$, $M = 0.1$, and $S = 2.4$. It is found that $f'(\eta)$ escalates due to the enlarging value of A for the first solution but not for the second solution. Meanwhile, $\theta(\eta)$ reduces with the enlarging value of A for both solutions.

Figures 12 and 13 show the impact of several values of S on $f'(\eta)$ and $\theta(\eta)$, when $\phi_{s1} = \phi_{s2} = 0.01$, $\beta = 0.02$, $\lambda = -1$, $A = B = 0.2$, and $M = 0.1$. It is found that $f'(\eta)$ escalates due to the enlarging value of S except for the second solution. Meanwhile, $\theta(\eta)$ reduces with the enlarging value of S for both solutions hence, reducing the layer thickness at the boundary.

Figures 14 and 15 show the impact of several values of ϕ_{s2} on $f'(\eta)$ and $\theta(\eta)$, when $\phi_{s1} = 0.01$, $\beta = 0.02$, $\lambda = -1$, $A = B = 0.2$, $M = 0.1$, and $S = 2.4$. It is found that $f'(\eta)$ escalates due to the enlarging value of S for the first solution only and reversely for the other one. Meanwhile, $\theta(\eta)$ enhances with the enlarging value of ϕ_{s2} for both solutions.

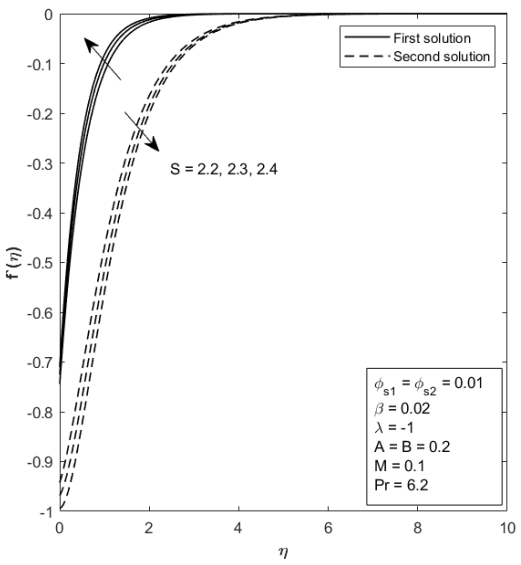

Fig. 12. Velocity profile for several S.

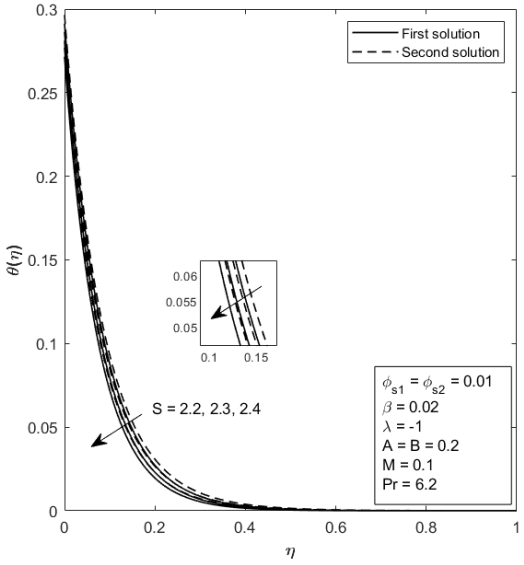

Fig. 13. Temperature profile for several S.

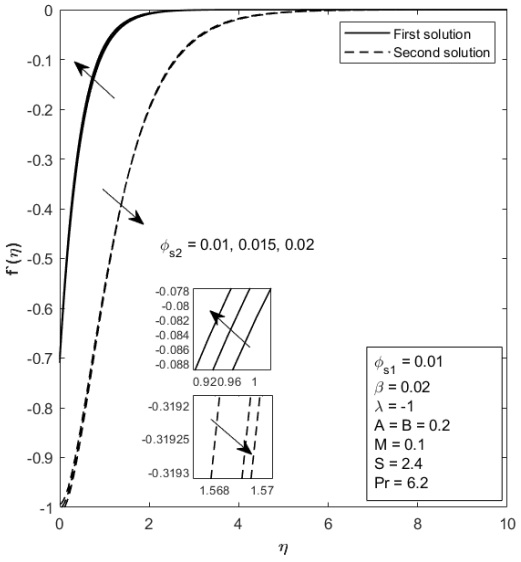

Fig. 14. Velocity profile for several ϕ_{s2}.

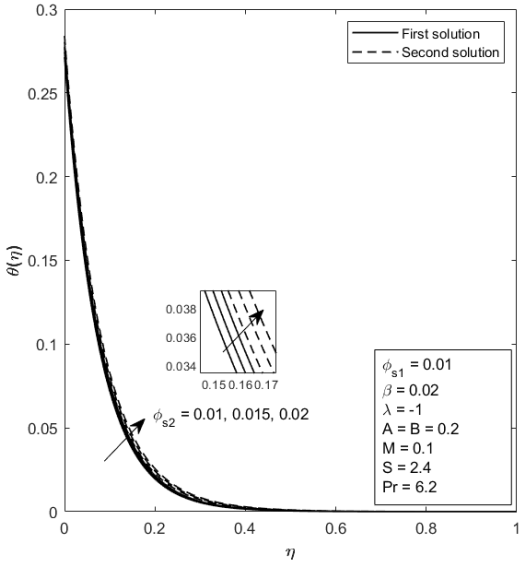

Fig. 15. Temperature profile for several ϕ_{s2}.

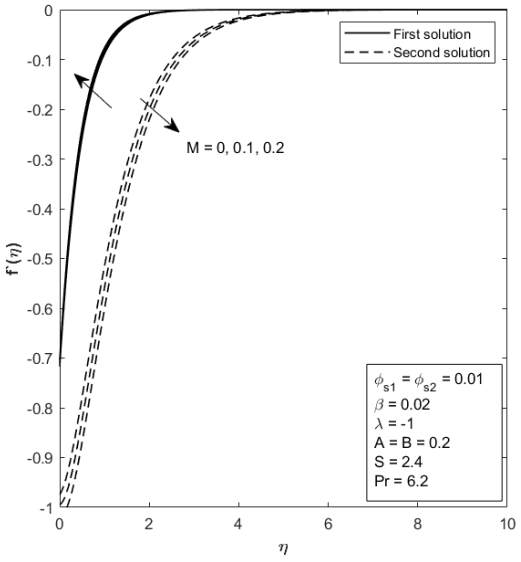

Fig. 16. Velocity profile for several M.

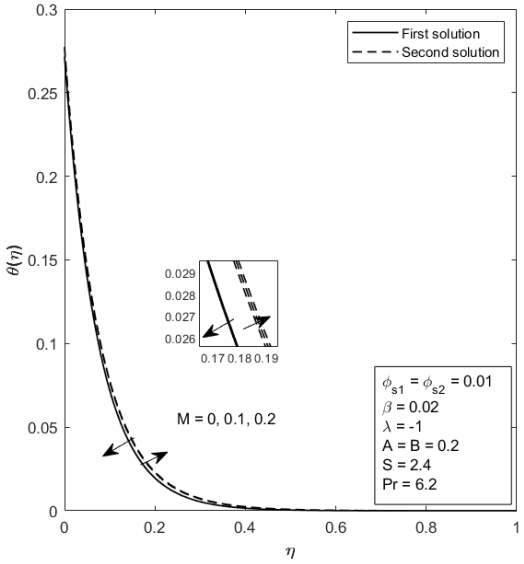

Fig. 17. Velocity profile with several M.

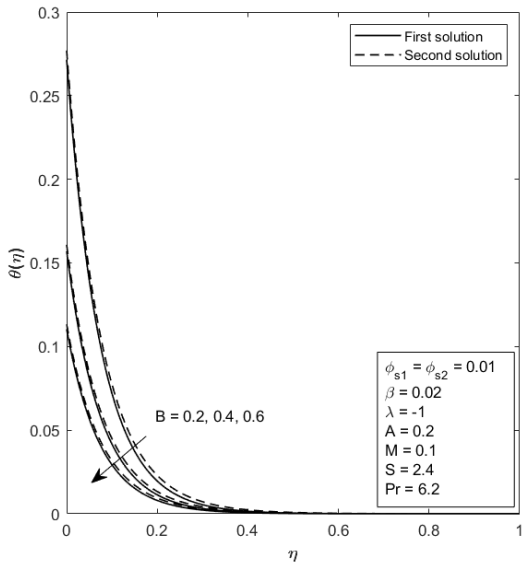

Fig. 18. Temperature profile with several B.

Figures 16 and 17 show the impact of several values of M on $f'(\eta)$ and $\theta(\eta)$, when $\phi_{s1} = \phi_{s2} = 0.01$, $\beta = 0.02$, $\lambda = -1$, $A = B = 0.2$, and $S = 2.4$. As the value of M enhances, $f'(\eta)$ escalates for the first solution but differs from the second solution. Meanwhile, the value of $\theta(\eta)$ decreases for the first solution and vice versa with the second solution with the enlarging value of M.

Figure 18 shows the impact of several values of B on $\theta(\eta)$, when $\phi_{s1} = \phi_{s2} = 0.01$, $\beta = 0.02$, $\lambda = -1$, $A = 0.2$, $M = 0.1$, and $S = 2.4$. It is found that $\theta(\eta)$ reduces with the enlarging values of B for both solutions and decaying the thermal layer thickness.

4. Conclusion

This numerical study has been examined for the magnetohydrodynamic hybrid nanofluid flow over a stretchable/shrinkable sheet with heat source and slip. This problem was solved numerically in MATLAB software. In the present results, the solutions for $S > S_c$ and $\lambda > \lambda_c$ are found to be dual and not unique. Furthermore, it is deduced that the shrinking sheet gives dual solutions at a specific limit and the stretch sheet gives most of the one unique solutions. With the implementation of heat source, suction, velocity slip, and thermal slip, the first solution simulates that:

— The skin friction coefficient can be augmented by enlarging the magnetic parameter during the sheet is shrunk but not during the sheet is stretched;
— The local Nusselt number can be augmented by enlarging the magnetic parameter especially when the sheet is shrunk;
— The velocity profile is escalated when the magnetic parameter increases but oppositely for the temperature profile.

And the second solution simulates that:

— The skin friction coefficient and the local Nusselt number can be augmented by reducing the magnetic parameter either when the sheet is shrunk or stretched;
— The velocity profile is escalated when the magnetic parameter is decayed but reversibly to the temperature profile.

The reliability of these solutions has been proven by the previous studies that deduced only the first solution gives the reliable solution. Even so, the second solution still can be used for reference in future studies. Nonetheless, it is crucial to acknowledge that the present findings can only be deemed reliable within the confines of the specified model description and geometry.

[1] Choi S. U. S. Enhancing thermal conductivity of fluids with nanoparticles. In: Proceedings of the 1995 ASME International Mechanical Engineering Congress and Exposition, FED. 99–106 (1995).

[2] Taylor R., Coulombe S., Otanicar T., Phelan P., Gunawan A., Lv W., Rosengarten G., Prasher R., Tyagi H. Small particles, big impacts: A review of the diverse applications of nanofluids. Journal of Applied Physics. **113** (1), 011301 (2013).

[3] Devendiran D. K., Amirtham V. A. A review on preparation, characterization, properties and applications of nanofluids. Renewable and Sustainable Energy Reviews. **60**, 21–40 (2016).

[4] Babu J. A. R., Kumar K. K., Rao S. S. State-of-art review on hybrid nanofluids. Renewable and Sustainable Energy Reviews. **77**, 551–565 (2017).

[5] Wahid N. S., Arifin N. M., Khashi'ie N. S., Pop I., Bachok N., Hafidzuddin E. H. MHD hybrid nanofluid flow with convective heat transfer over a permeable stretching/shrinking surface with radiation. International Journal of Numerical Methods for Heat & Fluid Flow. **32** (5), 1706–1727 (2022).

[6] Khashi'ie N. S., Waini I., Wahid N. S., Arifin N. M., Pop I. Unsteady separated stagnation point flow due to an EMHD Riga plate with heat generation in hybrid nanofluid. Chinese Journal of Physics. **81**, 181–192 (2023).

[7] Yahaya R. I., Arifin N. M., Pop I., Ali F. M., Isa S. S. P. M. Dual solutions of unsteady mixed convection hybrid nanofluid flow past a vertical Riga plate with radiation effect. Mathematics. **11** (1), 215 (2023).

[8] Hamzah M. H., Sidik N. A. C., Ken T. L., Mamat R., Najafi G. Factors affecting the performance of hybrid nanofluids: A comprehensive review. International Journal of Heat and Mass Transfer. **115** (A), 630–646 (2017).

[9] Eshgarf H., Kalbasi R., Maleki A., Shadloo M. S., Karimipour A. A review on the properties, preparation, models and stability of hybrid nanofluids to optimize energy consumption. Journal of Thermal Analysis and Calorimetry. **144**, 1959–1983 (2021).

[10] Waini I., Ishak A., Pop I. Hybrid nanofluid flow induced by an exponentially shrinking sheet. Chinese Journal of Physics. **68**, 468–482 (2020).

[11] Wahid N. S., Arifin N. M., Khashi'ie N. S., Pop I. Hybrid nanofluid slip flow over an exponentially stretching/shrinking permeable sheet with heat generation. Mathematics. **9** (1), 30 (2021).

[12] Mahabaleshwar U. S., Aly E. H., Anusha T. MHD slip flow of a Casson hybrid nanofluid over a stretching/shrinking sheet with thermal radiation. Chinese Journal of Physics. **80**, 74–106 (2022).

[13] Mahesh R., Mahabaleshwar U. S., Kumar P. N. V., Öztop H. F., Abu-Hamdeh N. Impact of radiation on the MHD couple stress hybrid nanofluid flow over a porous sheet with viscous dissipation. Results in Engineering. **17**, 100905 (2023).

[14] Wahid N. S., Arifin N. M., Khashi'ie N. S., Pop I. Mixed convection MHD hybrid nanofluid over a shrinking permeable inclined plate with thermal radiation effect. Alexandria Engineering Journal. **66**, 769–783 (2023).

[15] Jaafar A., Jamaludin A., Mohd Nasir N. A. A., Nazar R., Pop I. MHD opposing flow of Cu–TiO_2 hybrid nanofluid under an exponentially stretching/shrinking surface embedded in porous media with heat source and slip impacts. Results in Engineering. **17**, 101005 (2023).

[16] Patel V. K., Pandya J. U., Patel M. R. Testing the influence of TiO_2–Ag/water on hybrid nanofluid MHD flow with effect of radiation and slip conditions over exponentially stretching & shrinking sheets. Journal of Magnetism and Magnetic Materials. **572**, 170591 (2023).

[17] Mandal G., Pal D. Stability analysis of radiative-magnetic hybrid nanofluid slip flow due to an exponentially stretching/shrinking permeable sheet with heat generation. International Journal of Ambient Energy. **44** (1), 1349–1360 (2023).

[18] Takabi B., Salehi S. Augmentation of the heat transfer performance of a sinusoidal corrugated enclosure by employing hybrid nanofluid. Advances in Mechanical Engineering. **6**, 147059 (2015).

[19] Oztop H. F., Abu-Nada E. Numerical study of natural convection in partially heated rectangular enclosures filled with nanofluids. International Journal of Heat and Fluid Flow. **29** (5), 1326–1336 (2008).

[20] Wahid N., Arifin N., Khashi'ie N., Pop I., Bachok N., Hafidzuddin M. Radiative flow of magnetic nanofluids over a moving surface with convective boundary condition. Mathematical Modeling and Computing. **9** (4), 791–804 (2022).

[21] Norzawary N., Bachok N., Ali F., Rahmin N. Double solutions and stability analysis of slip flow past a stretching/shrinking sheet in a carbon nanotube. Mathematical Modeling and Computing. **9** (4), 816–824 (2022).

[22] Yahaya R., Ali F., Arifin N., Khashi'ie N., Isa S. S. P. M. MHD flow of hybrid nanofluid past a stretching sheet: double stratification and multiple slips effects. Mathematical Modeling and Computing. **9** (4), 871–881 (2022).

Вплив магнітогідродинаміки на гібридний потік нанофлюїдів із ковзанням і джерелом тепла над експоненціально розтягуваним/усаджуваним проникним листом

Радзі Н. А. М.[1], Вахід Н. С.[1], Сом А. Н. М.[3], Аріфін Н. М.[1,2]

[1] *Кафедра математики та статистики природничого факультету, Університет Путра Малайзії, 43400 UPM Серданг, Селангор, Малайзія*
[2] *Інститут математичних досліджень, Університет Путра Малайзії, 43400 UPM Серданг, Селангор, Малайзія*
[3] *Центр фундаментальних досліджень сільськогосподарських наук, Університет Путра Малайзії, 43400 UPM Серданг, Селангор, Малайзія*

У цьому дослідженні розглядається гібридний потік нанофлюїду глинозем–мідь/вода через проникний лист, враховуючи ковзання, магнітогідродинаміку та джерело тепла. Для аналізу системи модель перетворюється на нелінійні звичайні диференціальні рівняння (ODEs) за допомогою перетворення подібності. Чисельні розв'язки досягаються за допомогою реалізації функції bvp4c в MATLAB. Аналізуються профілі швидкості та температури, локальне поверхневе тертя та число Нуссельта для різних параметрів. Крім того, досліджується вплив магнітогідродинаміки на систему. Збільшення магнітного параметра призводить до збільшення товщини прикордонного шару та підвищення коефіцієнта поверхневого тертя. Загалом, це дослідження проливає світло на складну поведінку потоків гібридних нанофлюїдів і дає цінну інформацію про вплив ковзання, магнітогідродинаміки та джерела тепла на модель, а також представляє перевірену модель, що демонструє переконливе посилення теплопередачі за рахунок включення міді в нанорідину оксиду алюмінію.

Ключові слова: *магнітогідродинамічний; гібридна нанофлюїд; джерело тепла; розтягнення/усадження.*